Nuclear structure study of ^{26}Mg following heavy-ion-induced fusion-evaporation reaction

S. S. Bhattacharjee, R. Bhattacharjee, R. Chakrabarti,* R. Raut,† S. S. Ghugre, and A. K. Sinha
UGC-DAE Consortium for Scientific Research, Kolkata Centre, Kolkata 700098, India

T. Trivedi and L. Chaturvedi
Guru Ghasidas University, Bilaspur 495009, India

S. Saha, J. Sethi, and R. Palit
Tata Institute of Fundamental Research, Mumbai 400005, India

(Received 25 October 2013; revised manuscript received 10 February 2014; published 28 February 2014)

Nuclear structure of the ^{26}Mg nucleus has been probed, for the first time, using heavy-ion-induced fusion-evaporation reaction and a large array of high-resolution γ-ray detectors (Clovers). The level structure of the nucleus reported in the earlier studies, using light-ion reactions, has been re-examined and new transitions have been identified. Existing spin-parity assignments have been confirmed and new assignments have been made from anisotropy and polarization measurements. Large basis shell-model calculations, involving cross-shell excitation-have been carried out, for the first time, in ^{26}Mg as well as in the neighboring isotopes and the agreement with the experimental level energies is rather remarkable.

DOI: 10.1103/PhysRevC.89.024324 PACS number(s): 23.20.Lv, 21.10.Hw, 21.60.Cs, 27.30.+t

I. INTRODUCTION

The spherical shell-model approach fails to interpret the structural data for the neutron-rich nuclei in the islands of inversion [1]. The observations at the island of inversion have been ascribed to an inverted level structure with the intruder single-particle states from a higher-lying shell falling below the normally lower-lying shell states [2,3]. The nuclei in the transient region between the line of β stability and the island of inversion carry the signatures of evolving nuclear structure showing departures from the shell-model picture. For the island of inversion near $N = 20$, a number of studies have been reported for nuclei in the associated transient region. The Mg nuclei belonging to this transitional region have attracted a host of experimental and theoretical investigations covering the ground-state properties and the spectroscopic behavior of the excited states. The spectroscopic investigations of these nuclei are almost entirely based on the direct nuclear reactions (with limited access to the high spin domain) involving stable or radioactive ion beams for the population of the excited states while using only a few γ detectors with low-efficiency/low-resolution [Ge(Li)/NaI(Tl) detectors] [4,5]. Few of the reported γ-γ coincidence studies of the high spin structure for the isotopes of Mg using a fusion-evaporation reaction include the hard to reach ^{30}Mg nucleus by Deacon *et al.* [6] who have employed the reaction ^{18}O + ^{14}C and used the GAMMASPHERE coupled with FMA and have only limited statistics due to very low cross section for the reaction used. Yet another investigation by Seweryniak *et al.* [7] addressed the neutron deficient isotope of ^{22}Mg, populated using the ^{12}C + ^{12}C fusion-evaporation reaction along with the GAMMASPHERE used as the detection system.

The isotopic chain of Mg, as observed in the aforesaid studies, exhibit evolving structural characteristics (changes in shape as well as deformation) as a function of neutron number. The $N = Z$, ^{24}Mg isotope displays a deformed ground state. Further addition of neutrons leads to quite rapid changes in the shape, deformation, and spin structure. The next even-even Mg isotope, ^{26}Mg displays shape coexistence indicating both a prolate and an oblate minima corroborating a highly transitional behavior assigned to it. The calculations using constrained Hartree-Fock-Bogoliubov + quasi-particle random phase approximation (QRPA) model demonstrate the β and γ-soft character of the nucleus [8]. The present work reports, for the first time, a γ-γ coincidence spectroscopic study of the ^{26}Mg nucleus using heavy-ion-induced fusion-evaporation reaction involving ^{13}C + ^{18}O employing a large array of γ-ray detectors (Clovers). Further, large basis shell-model calculations involving cross-shell excitations have been carried out for ^{26}Mg and the neighboring isotopes to gauge the evolving shell structure in this region.

II. EXPERIMENTAL DETAILS AND DATA ANALYSIS

High spin states of ^{26}Mg have been populated utilizing the reaction ^{13}C + ^{18}O, with ^{13}C beam of energy 30 MeV provided by the BARC-TIFR Pelletron Linac facility at Mumbai. The neutron rich ^{18}O target was prepared by heating a 50-mg/cm^2-thick Ta foil in an atmosphere of enriched ^{18}O to form Ta_2O_5. The total equivalent thickness of ^{18}O was estimated to be $\sim$1.6 mg/cm^2 considering both the sides of Ta foil. The thickness of the Ta foil was sufficient to stop the beam and hence the reaction occurred only on the side facing the beam while the ^{18}O layer on the opposite side (away from the beam) did not contribute to the reaction. The de-excited γ rays are detected with the help of Indian National Gamma Array (INGA) which at the time of the present experiment consisted of 15 Compton suppressed Clover detectors. The distance from

*Present address: Nuclear Physics Division, Bhabha Atomic Research Centre, Mumbai 400085, India.
†rraut@alpha.iuc.res.in

the target to the front face of the detector is ≈24 cm. The Clover detectors are placed at 40°, 65°, 90°, −65°, −40°, −23° with respect to the beam direction. Two and higher fold Clover coincidence events are recorded with the help of digital data acquisition system based on the Pixie-16 modules by XIA LLC [9]. The energy calibration is carried out using source data and residue radioactivity. The energy calibration has been done using a polynomial of fourth degree and a square-root term, using the ROOT package [10] in view of the high-energy γ-ray transitions expected in the present experiment. The Clover detector, used in the addback mode, is optimized for such investigations due to its enhanced detection efficiency for high energy γ rays. The linear polarization measurements are feasible using Clover detectors, as any one of the four crystals may be used as the scatterer, with the remaining crystals acting as absorbers providing scattering yields both in the the perpendicular and parallel directions with respect to the reaction plane. The level scheme is developed from the observed coincidence relations. The conventional symmetric and angle dependent E_γ-E_γ matrices are constructed using MARCOS [11] and analyzed using the RADWARE [12] package. In total about 1.6 billion coincident events of fold 2 and higher were recorded.

A. Angular anisotropy

The information on the dominant multipolarity of the γ transition is obtained from the observed coincidence angular anisotropy. The method is detailed in Ref. [11] and is based on the determination of the coefficient for the directional correlation ($R_{\rm DCO}$) defined as

$$R_{\rm DCO} = \frac{I_{\gamma 1}(\text{at } \theta \text{ gated by } \gamma 2 \text{ at } 90^\circ)}{I_{\gamma 1}(\text{at } 90^\circ \text{ gated by } \gamma 2 \text{ at } \theta)}. \quad (1)$$

A calculation of $R_{\rm DCO}$ requires gates to be set on transitions observed both at 90° as well as on forward and/or backward angles. Many of the γ transitions of interest occur before the stopping of the recoils (stopping time ∼ hundreds of fs), with the energies of the emitted γ rays consequently exhibiting Doppler shifts thus making it difficult to set gates on these transitions at angles other than at 90°.

To circumvent this problem of determining the $R_{\rm DCO}$ values, a parameter termed as the anisotropy ratio [13], defined below, is used for assigning multipolarity of the observed γ transitions.

$$R_{\rm anisotropy} = \frac{I_{\gamma 1}(\text{at } 40^\circ \text{ gated by } \gamma 2 \text{ at } 90^\circ)}{I_{\gamma 1}(\text{at } 65^\circ \text{ gated by } \gamma 2 \text{ at } 90^\circ)}. \quad (2)$$

The anisotropy ratio ($R_{\rm anisotropy}$) for different transitions is extracted from matrices with 90° detectors on the x axis and detectors at particular angles (40°, 65°) on the y axis. The results for transitions of known multipolarity are shown in Fig. 1. The weighted average of the experimental $R_{\rm anisotropy}$ for dipole transitions has been found to be 0.95 (dipole gate) and 1.13 (quadrupole gate) while that for quadrupole transitions has been calculated to be 1.82 (dipole gate) and 1.68 (quadrupole gate). Lines corresponding to these values have been drawn (Fig. 1) to guide the eye. As is evident from the figure, the anisotropy method is able to distinguish

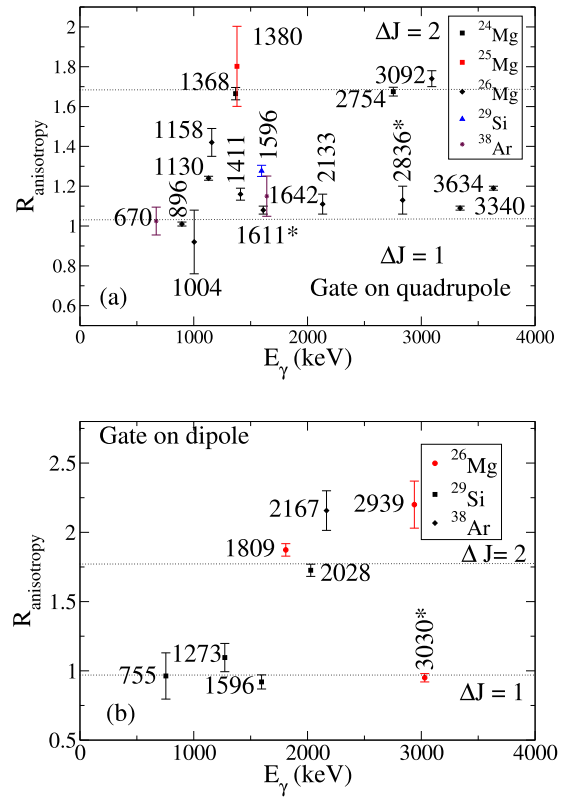

FIG. 1. (Color online) The experimental $R_{\rm anisotropy}$ values for transitions in ^{24,25,26}Mg, ^{29}Si, and ^{38}Ar. The newly identified γ rays in ^{26}Mg are marked with an asterisk.

between transitions of different multipolarities. The technique has been further validated by evaluating both the $R_{\rm anisotropy}$ and the $R_{\rm DCO}$ for strong transitions of known multipolarity and confirming that the multipolarities extracted from the two methods are in agreement. Figure 1 also shows results of $R_{\rm anisotropy}$ measurement for new transitions in the nucleus of interest ^{26}Mg.

Information on the multipolarity and mixing ratio of a γ transition can also be obtained from angular distribution measurement using singles data. The observed angular distribution is fitted using the equation below following the procedure in Ref. [14],

$$W(\theta) = 1 + A_2 P_2(\cos\theta) + A_4 P_4(\cos\theta). \quad (3)$$

The efficiency corrected angle dependent intensities are used to obtain the angular distribution coefficients A_2 and A_4. Figure 2 illustrates the fit to the angular distribution data for the 1130-keV ($2_2^+ \rightarrow 2_1^+$) transition in ^{26}Mg nucleus. The mixing ratio (δ) has been obtained following the prescription described by Singh *et al.* [14]. The χ^2 plot for the 1130-keV transition is also shown in Fig. 2. The resulting $\delta = 0.14 \pm 0.05$, following the convention of Rose and Brink, is in agreement with the reported value 0.12 ± 0.02 [14–17]. However, this procedure could not be applied to other transitions in ^{26}Mg owing to the contaminations from the other channels, Doppler effects, and sparse statistics.

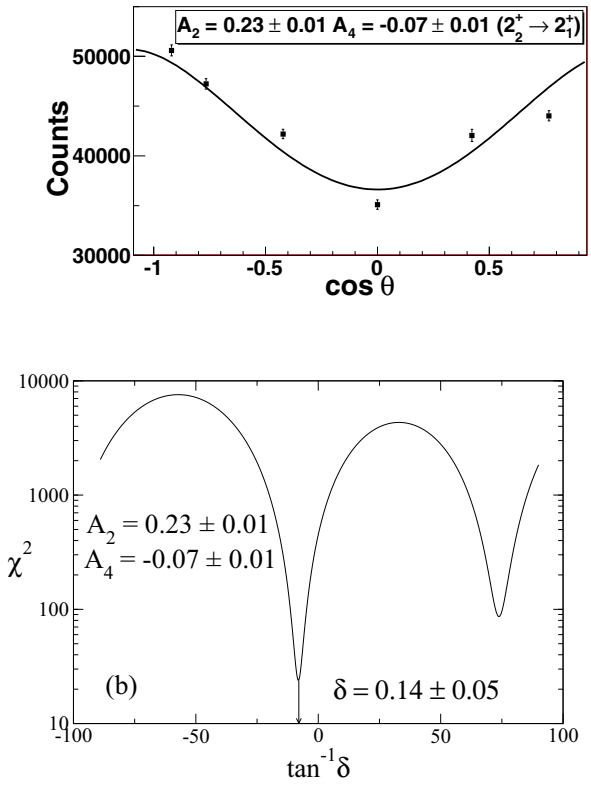

FIG. 2. (Color online) Angular distribution fit for 1130 keV ($2_2^+ \rightarrow 2_1^+$) transition in ^{26}Mg and the χ^2 analysis to obtain the corresponding mixing ratio.

B. γ-ray polarization

The use of Clover detectors uniquely facilitates the measurement of linear polarization of the observed γ-ray transitions which helps in determining its electromagnetic nature. Each crystal of the Clover detector acts as a scatterer and the adjacent two crystals as absorbers along the perpendicular and parallel direction, with respect to the reaction plane. The distinction between the electric and magnetic transition can be obtained from the observed asymmetry between the number of perpendicular and parallel Compton scattered events for a given γ transition. This asymmetry is defined as

$$\Delta_{\text{Pol}} = \frac{aN_\perp - N_\parallel}{aN_\perp + N_\parallel}, \tag{4}$$

where $N_\perp$ and $N_\parallel$ are the number of photons scattered in the perpendicular and the parallel direction respectively. The parameter "a" denotes a correction factor due to the asymmetry in the geometrical response of the Clover segments in the array. It is measured by using unpolarized γ-ray emission, and the following equation [18,19]:

$$a = \frac{N_\parallel}{N_\perp}. \tag{5}$$

The value of the asymmetry factor is energy dependent $[a(E_\gamma) = a_0 + a_1 E_\gamma]$ and the parameters a_0 and a_1 are determined using radioactive sources and beam-off radioactivity under identical experimental conditions (position, etc.) as the in-beam measurements. A representative energy dependence of a (for one Clover detector) up to $E_\gamma \sim 3$ MeV is presented in Fig. 3. The average value (over all the 90° detectors) of the fitting parameters are $a_0 = 1.003 \pm 0.002$ and $a_1 = 1.0 \pm 4.0 \times 10^{-6}$ (keV)$^{-1}$. Owing to the very small value of the a_1 coefficient ($\sim 10^{-6}$) it is expected to impact, if at all, the polarization values of only the very high-energy γ-ray transitions. In the present work, the quoted uncertainties on the polarization incorporate the uncertainties on the a_1 coefficient. The value of the Δ_{Pol} is extracted from the two asymmetric γ-γ matrices where the y axis contains the parallel (perpendicular) scattered events in detectors at 90° and the x axis contains the coincident events in all other detectors. Gates are applied on the x axis and counts corresponds to the parallel ($N_\parallel$) and the perpendicular ($N_\perp$) scattering are obtained from the resulting spectra. The value of Δ_{Pol} is indicative of the electromagnetic nature of the γ transition. For a pure electric transition Δ_{Pol} is positive while a negative value of Δ_{Pol} implies a magnetic transition. A near zero value of Δ_{Pol} is indicative of a mixed transition. Figure 4 depicts the Δ_{Pol} values for different γ-ray transitions observed in the current experiment. As is evident from the figure, we are able to distinguish the electromagnetic nature of the transition therefrom.

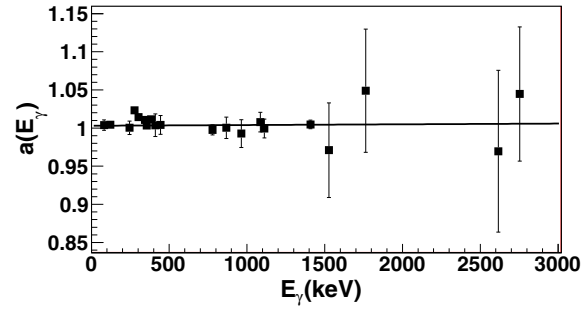

FIG. 3. (Color online) Plot of the asymmetry factor "a" as a function of γ-ray energy for the Clover detector placed at 90° with respect to the beam direction in the present setup.

The polarization asymmetry is related to the degree of linear polarization (P) by the following:

$$P = \frac{\Delta_{\text{Pol}}}{Q(E_\gamma)}, \tag{6}$$

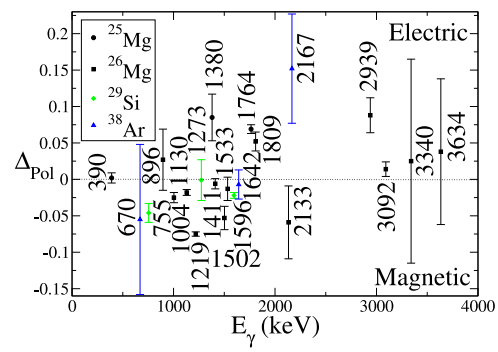

FIG. 4. (Color online) Plot of the polarization asymmetry for γ-ray transitions observed in the current experiment.

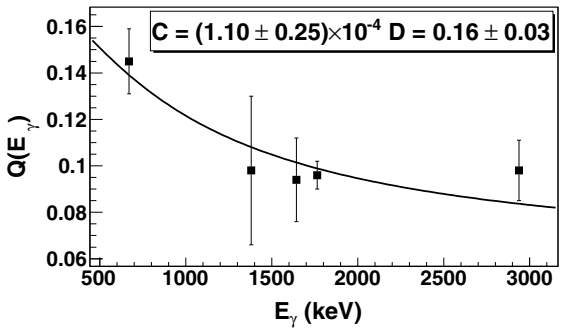

FIG. 5. (Color online) Plot of the polarization sensitivity as a function of γ-ray energy. The solid curve is obtained by fitting the data with Eq. (7).

where $Q(E_\gamma)$ [18,19] is the energy-dependent polarization sensitivity. Further,

$$Q(E_\gamma) = (CE_\gamma + D)Q_0(E_\gamma), \tag{7}$$

where

$$Q_0(E_\gamma) = \frac{(\alpha+1)}{(\alpha^2+\alpha+1)}, \tag{8}$$

with

$$\alpha = \frac{E_\gamma(MeV)}{0.511}, \tag{9}$$

The polarization sensitivity has been calculated for γ transitions of previously known multipolarity and mixing ratio following the prescription in Refs. [15,17,20]. Palit *et al.* [20] have obtained the energy dependence of the polarization sensitivity for a similar setup which has now been extended beyond 1.5 MeV, as shown in Fig. 5.

The extracted polarization (P) for γ-ray transitions observed in the present experiment is plotted in Fig. 6. The figure also includes the polarization of known transitions from other nuclei, populated in the current investigation, that are found to corroborate with the previous assignments. The procedure for calculating the theoretical polarization is outlined in Ref. [3]. The present calculations have been carried out with $\sigma/J = 0.3$, where σ is the width of the m-state (Gaussian) distribution. The theoretical polarization has been used to extract polarization

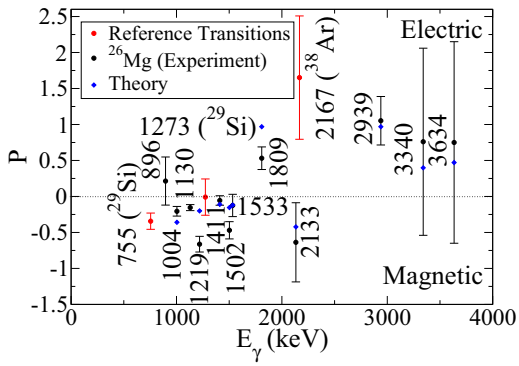

FIG. 6. (Color online) Plot of the experimental and calculated polarization for γ-ray transitions observed in the present work.

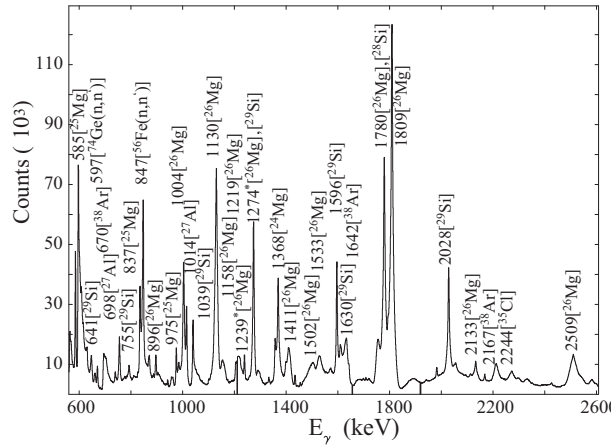

FIG. 7. Projection spectrum illustrating the nuclei populated in the present experiment. The new transitions belonging to ^{26}Mg have been labeled with an asterisk.

sensitivity [Eq. (6) and Fig. 5] and for subsequent comparison with the experimental results (Fig. 6). The calculated values are in qualitative agreement with the experimental results, as illustrated in Fig. 6.

III. LEVEL SCHEME OF ^{26}Mg

Previous investigations on the study of the level structure of ^{26}Mg were carried out using light-ion-induced reactions. The present investigation reports the first heavy-ion-induced high-resolution γ-ray spectroscopy measurement on ^{26}Mg. The projection spectrum as obtained from the γ-γ matrix is depicted in Fig. 7. From the characteristic γ-ray transitions, the nuclei populated in the present experiment have been identified to include ^{24,25,26}Mg, ^{27}Al, and ^{28,29}Si, as labeled in the figure. The γ-ray transitions attributed to nuclei such as ^{38}Ar and ^{35}Cl originate from the ^{13}C beam interacting with the ^{27}Al target holder.

The level scheme of the ^{26}Mg nucleus from this work, based on γ-γ coincidence measurements, is presented in Fig. 8. The projected spectra for the emissions in the forward angle, 90°, and the backward angle with a gate on the 1809-keV transition (from the first 2^+ state to the 0^+ ground state) are presented in Fig. 9. The spectra illustrates line shapes and Doppler shifts for various transitions that may be used for extracting the level lifetimes. Several of the γ transitions, reported in the earlier direct reaction based studies, are not observed in the present experiment, which uses fusion-evaporation reaction, and hence are not placed in the level scheme. The spin-parity assignment of some of the levels observed in the present experiment have not been possible due to limited statistics and we have used previously reported assignments in such cases (Ref. [21]). Around eight new transitions of ^{26}Mg have been identified in the present work and have been placed based on the observed coincidence conditions. The relative intensities of the transitions have been calculated after due incorporation of the efficiency characteristics of a Clover detector to an extended energy range up to ∼6 MeV, using data from Ref. [22]. The level and transition energies, $R_{\text{anisotropy}}$, and

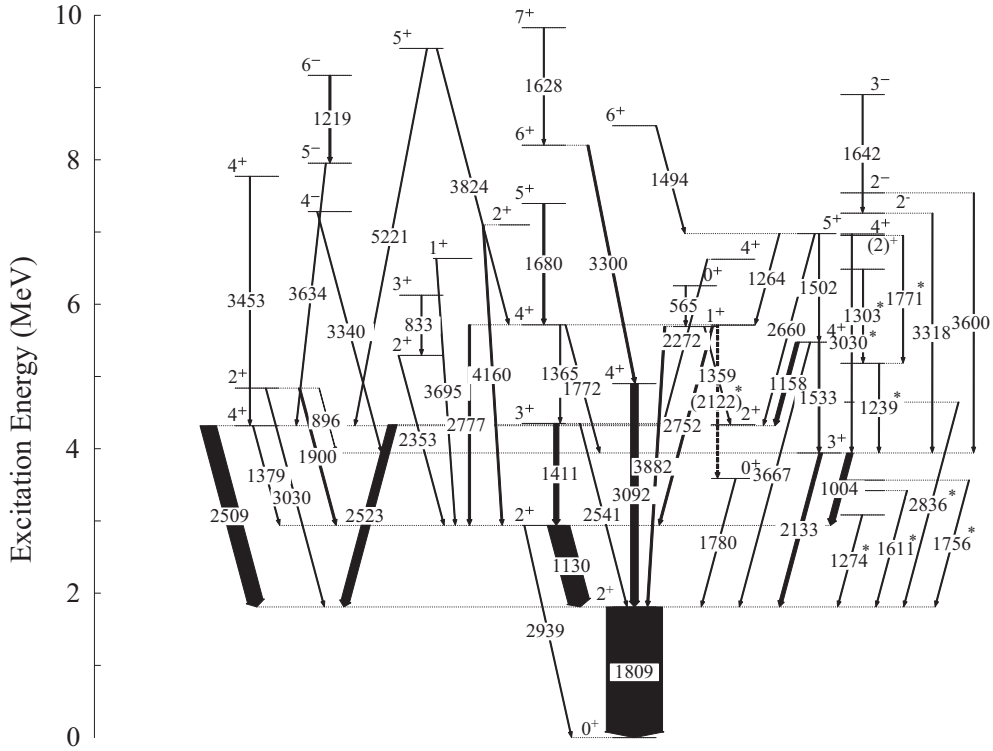

FIG. 8. Level scheme of ^{26}Mg nucleus from the present work. New transitions are indicated by asterisk. The widths of the arrows connecting the levels are proportional to the γ-ray intensities.

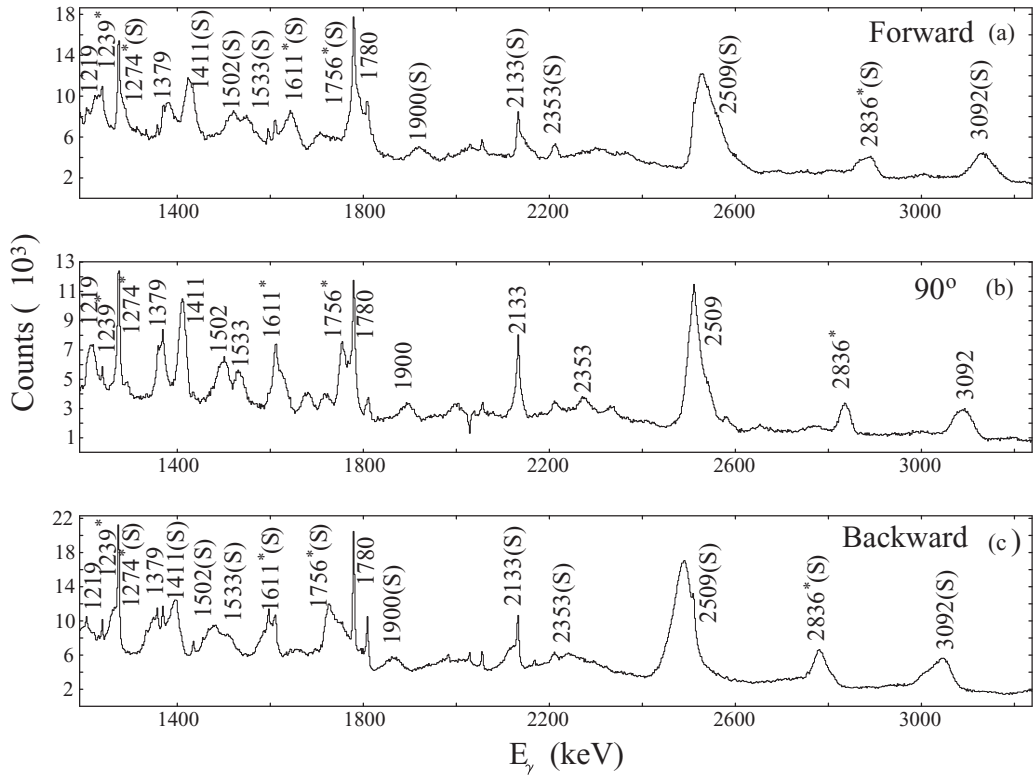

FIG. 9. Angle dependent coincidence spectra with gate set on the 1809-keV transition in ^{26}Mg, illustrating the observed Doppler shapes and shifts for different γ-ray transitions. Completely shifted transitions and the transitions with Doppler shapes are identified with the label "S"at the forward and backward angles. The new transitions have been labeled with an asterisk.

TABLE I. Details of γ-ray transitions of the ^{26}Mg nucleus, observed in the present work.

E_i (keV)	E_γ (keV)	E_f (keV)	I_γ (%)	J_i^π	J_f^π	$R_{\text{anisotropy}}$	P	Assignment
1809	1809.2 ± 1.0	0	259.3 ± 10.2	2_1^+	0_1^+	1.87 ± 0.04[a]	0.53 ± 0.15	E2
2939	1130.4 ± 0.3	1809	100.0 ± 7.3	2_2^+	2_1^+	1.24 ± 0.01[b]	–0.15 ± 0.04	M1 + E2
	2938.9 ± 1.0	0		2_2^+	0_1^+	2.20 ± 0.17[a]	1.05 ± 0.33	E2
3083	1274.1 ± 2.0	1809			2_1^+			
3420	1611.4 ± 1.7	1809			2_1^+	1.08 ± 0.02[b]		D + Q
3565	1756.1 ± 1.9	1809			2_1^+			
3589	1779.6 ± 2.1	1809		0_2^+	2_1^+	2.19 ± 1.46[b]	1.74 ± 2.80	E2
3943	1004.1 ± 1.6	2939	29.3 ± 7.6	3_1^+	2_2^+	0.92 ± 0.16[b]	–0.20 ± 0.06	M1 + E2
	2133.1 ± 1.0	1809	17.1 ± 2.7	3_1^+	2_1^+	1.11 ± 0.05[b]	–0.63 ± 0.55	M1(+ E2)
4318	1379.2 ± 1.1	2939		4_1^+	2_2^+			
	2509.0 ± 2.0	1809	73.3 ± 20.6	4_1^+	2_1^+		1.2 ± 1.6	(E2)[c]
4332	2523.0 ± 2.0	1809	40.4 ± 52.7	2_3^+	2_1^+		–0.57 ± 0.61	
4350	1411.4 ± 0.4	2939	24.0 ± 3.0	3_2^+	2_2^+	1.16 ± 0.03[b]	–0.05 ± 0.06	M1 + E2
	2541.0 ± 2.0	1809		3_2^+	2_1^+		–0.34 ± 0.91	M1 + E2[c]
4645	2836.0 ± 1.3	1809			2_1^+	1.13 ± 0.07[b]		D + Q
4839	896.0 ± 1.3	3943	2.1 ± 2.2	2_4^+	3_1^+	1.01 ± 0.01[b]	0.21 ± 0.33	M1 + E2
	1900.1 ± 2.0	2939	10.0 ± 2.7	2_4^+	2_2^+			M1(+ E2)[c]
	3030.0 ± 2.0	1809		2_4^+	2_1^+			
4901	3092.0 ± 2.0	1809	35.3 ± 3.4	4_2^+	2_1^+	1.74 ± 0.04[b]	0.17 ± 0.12	E2(+ M3)
5182	1238.9 ± 0.7	3943			3_1^+			
5292	2353.0 ± 2.0	2939		2_5^+	2_2^+			
5476	1158.3 ± 1.2	4318	18.6 ± 3.2	4_3^+	4_1^+	1.42 ± 0.07[b]		M1 + E2[c]
	1533.4 ± 0.8	3943	8.0 ± 2.7	4_3^+	3_1^+	1.19 ± 0.83[b]	–0.12 ± 0.15	M1 + E2
	3667.0 ± 2.0	1809		4_3^+	2_1^+			(E2)[c]
5691	1359.4 ± 0.3	4332		1_1^+	2_3^+			
	2752.0 ± 2.0	2939		1_1^+	2_2^+			
	3882.0 ± 2.0	1809		1_1^+	2_1^+			
5711	2122.5 ± 0.8	3589			0_2^+			
5715	1365.0 ± 1.1	4350		4_4^+	3_2^+			M1 + E2[c]
	1772.0 ± 1.1	3943		4_4^+	3_1^+			M1 + E2[c]
	2777.0 ± 2.0	2939		4_4^+	2_2^+			(E2)[c]
6125	833.1 ± 1.3	5292		3_3^+	2_5^+			
6256	565.1 ± 1.3	5691		0_4^+	1_1^+			D[c]
6485	1302.7 ± 1.3	5182						
6622	2271.8 ± 1.0	4350		4_5^+	3_2^+			
6634	3695.0 ± 2.0	2939		1_2^+	2_2^+			
6953	1771.1 ± 1.4	5182		$(2)_7^+$				
6973	3030.0 ± 2.0	3943		4_6^+	3_1^+	0.95 ± 0.03[a]		D + Q
6978	1263.7 ± 2.1	5715		5_1^+	4_4^+			
	1501.8 ± 1.0	5476		5_1^+	4_3^+	0.6 ± 0.8[b]	–0.47 ± 0.12	M1 + E2
	2660.0 ± 2.0	4318		5_1^+	4_1^+			M1 + E2[c]
7099	4160.0 ± 2.0	2939	8.6 ± 2.5	2_8^+	2_2^+			
7261	3318.0 ± 2.0	3943		2_1^-	3_1^+			(E1)[c]
7283	3340.0 ± 2.0	3943		4_1^-	3_1^+	1.09 ± 0.01[b]	0.75 ± 1.30	E1
7395	1680.0 ± 1.0	5715		5_2^+	4_4^+			M1 + E2[c]
7543	3600.0 ± 2.0	3943		2_2^-	3_1^+			(E1)[c]
7771	3453.0 ± 2.0	4318		4_7^+	4_1^+			
7952	3634.0 ± 2.0	4318		5_1^-	4_1^+	1.19 ± 0.01[b]	0.75 ± 1.40	E1 + M2

TABLE I. (*Continued.*)

E_i (keV)	E_γ (keV)	E_f (keV)	I_γ (%)	J_i^π	J_f^π	$R_{\text{anisotropy}}$	P	Assignment
8201	3300.0 ± 2.0	4901		6_1^+	4_2^+			E2(+ M3)[c]
8472	1494.0 ± 1.4	6978		6_2^+	5_1^+			M1 + E2[c]
8903	1642.3 ± 0.7	7261		3_2^-	2_1^-			
9171	1218.7 ± 2.3	7952	9.5 ± 2.7	6_1^-	5_1^-		−0.66 ± 0.10	M1 + E2[c]
9539	3824.0 ± 2.0	5715		5_5^+	4_4^+			
	5221.0 ± 2.0	4318		5_5^+	4_1^+			D + Q[c]
9829	1628.3 ± 1.2	8201		7_1^+	6_1^+			M1(+ E2)[c]

[a]From dipole gate.
[b]From quadrupole gate.
[c]Adopted from NNDC.

polarization of the γ-ray transitions and the consequent spin-parity assignments of the levels observed in the present study are summarized in Table I. The γ-transition energies below ∼2 MeV have been quoted with an uncertainty of ∼1 keV while those for higher energy transitions, with substantial Doppler broadening, have been assigned an uncertainty of 2 keV. The subsequent discussion shall detail the observations and assignments pertaining to the construction of the reported level scheme.

A. Negative-parity states

The negative-parity states are of particular importance owing to the associated cross-shell excitations from *sd* to the *pf* shell or from the lower *p* shell to *sd* shell. The excitation energy of the first negative-parity level could provide an indication of the relevant shell gap. The negative-parity levels 7261 [$J^\pi = (2,3)^-$], 7283 ($J^\pi = 4^-$), 7543 ($J^\pi = 2^-$), 7952 ($J^\pi = 5^-$), 8903 ($J^\pi = 3^-$), 9171 ($J^\pi = 6^-$), previously reported by Glatz *et al.* [4], have been observed in the present work. The 7261-keV level was tentatively assigned $J^\pi = (2,3)^-$ of which the $J^\pi = 2^-$ assignment has been concluded in the present study from shell-model calculations, discussed in the next section. It is noteworthy to mention that the lowest negative-parity state at 6876 keV ($J^\pi = 3^-$) could not be confirmed in the present investigation.

The anisotropy and polarization measurements aided in the spin-parity assignment of the observed levels that are in general agreement with the previous results. The 7283-keV level was reported to de-excite via 3340-keV and 2965-keV γ transitions. The 3340-keV transition has been observed in the present work and included in the proposed level scheme, while the 2965-keV transition has not been observed. The 3340-keV transition has been identified as an $E1$ transition, based on $R_{\text{anisotropy}}$ and polarization values, that corroborates with the previous assignment. The 7543-keV level was previously reported to be de-exciting by 3209, 4601, 3600, and 3191-keV transitions, of which only the 3600-keV transition has been confirmed in the present work. The 7952-keV (5^-) level was reported to de-excite by the 3634- and 2238-keV transitions, of which only the 3634-keV transition has been observed and found to be of dominant $E1$ character. The 9171 (6^-)-keV level was reported [4] to de-excite by 1216-, 1774-, and 1886-keV transitions. In the present work, only the 1216-keV, identified as 1219 keV, transition has been observed and included in the level scheme. This transition has been assigned a magnetic nature, based on the observed polarization asymmetry, thus confirming the previous assignment. The observation of 1774-keV transition could not be confirmed due to overlap from a strong 1780-keV transition, both from ^{26}Mg as well as from ^{28}Si. The 1886-keV transition has also not been observed in the present experiment. Most of the negative-parity states observed are yrast and the structure of these states have been probed from shell-model calculations, for the first time, as detailed in the following section.

B. Positive-parity states

The earlier researchers have discussed the positive-parity sequences in great detail [4,5], including the assignment of the experimental levels to rotational bands. Most of these levels up to $E_x \sim 10$ MeV have been observed. It is intriguing to observe several non-yrast positive-parity states (for instance, up to seven 2^+ and 4^+ levels, multiple 3^+, 5^+, 6^+ states have been observed) populated through fusion-evaporation reaction. It is observed that fusion-evaporation reactions preferentially populate yrast states, as noted by several researchers, for instance Scheck *et al.* [23].

Two of the new levels following the present study are 6973 and 6953 keV de-excited by 3030- and 1771-keV transitions, respectively. The $R_{\text{anisotropy}}$ value for the 3030-keV transition, with gate set on a dipole transition, is 0.95 ± 0.03, which indicates that this transition has a dominant dipole nature. Accordingly, the level at 6973 keV has been assigned a spin $J = 4$. Further, a positive parity has been assigned to this level based on the predictions of the shell-model calculations. The other new level at 6953 keV has been tentatively identified as the 2^+ state from correspondence to the shell-model calculated energy.

As far as the 2^+ states are concerned, Glatz *et al.* have reported up to five levels along with the corresponding shell-model calculated energies. In addition they have also observed a 2^+ state at 7099 keV, but have not reported a corresponding state from the shell-model calculations. In the present work, the first five 2^+ states have been found to comply with the results from Glatz *et al.* However, the sixth 2^+ level at 6745 keV

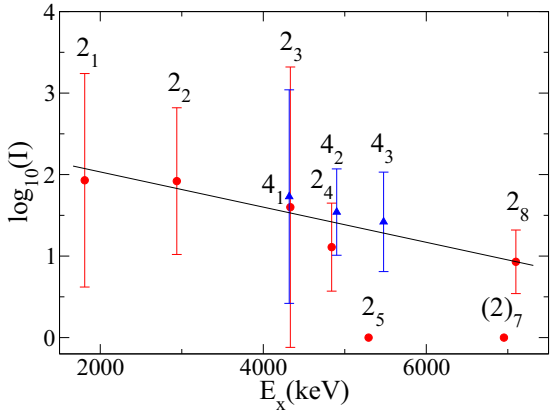

FIG. 10. (Color online) Yield of the 2^+ and 4^+ states in ^{26}Mg, populated in the present experiment. The solid line represents the slope in the yield of the 2^+ states.

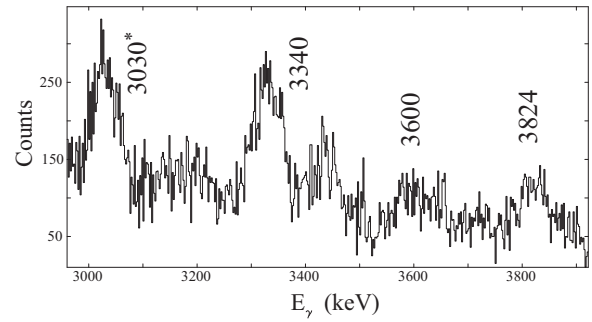

FIG. 11. Part of the coincidence spectrum at 90° with gate set on the 1004-keV transition. The new transition have been marked with an asterisk. This spectrum illustrates the observed Doppler broadening.

could not be confirmed in the present investigation. The level at 6953 keV has been tentatively assigned as the seventh 2^+ level. Further, the 2^+ level at 7099 keV has been well reproduced as the eighth 2^+ state in the shell-model calculations, discussed in the next section. It is worth mentioning that the yields of the 2^+ states, corrected for the cascade feeding from the upper levels, exhibit a general decreasing trend (Fig. 10) with increasing excitation energies, that may be attributed to the decreasing phase space.

In the ground-state band, similar to Glatz *et al.*, the 1809-, 4901-, and 8472-keV levels have been observed in the present work along with most of the associated γ transitions. For the second $K^\pi = 0^+$ band based on the 3589-keV (0^+) level, proposed by Glatz *et al.* [4] to be comprised of 3589-, 4332-, 6622-, and 9383-keV levels, only the first three of these levels have been observed in this work while none of the intraband $E2$ transitions could be confirmed from the present measurements. The $K^\pi = 3^+$ band was proposed to consist of 3941- (identified as 3943 in the current work), 5476-, 6978-, and 9112-keV levels, of which the first three have been observed along with the intraband transitions. The 1533- and 1502-keV transitions respectively de-exciting the 5476- and 6978-keV levels, shown in the 1809-keV gated spectrum in Fig. 9 have been assigned an $M1/E2$ character from the anisotropy and polarization measurements in the present work and are in agreement with the previous assignments.

One of the $K^\pi = 2^+$ bands, assigned by Glatz *et al.* [4], is comprised of 2939- (band head), 4350-, 5715-, 7395-, 8201-, 9829-, and 12 479-keV levels of which all, except 12 479 keV, have been observed in the present experiment. However, yield of only the 1411-keV intraband transition, de-exciting the 4350-keV level, is observed to be sufficiently strong for determination of anisotropy and polarization asymmetry wherefrom it has been assigned $M1/E2$ character, in agreement with the previous assignment. A second $K^\pi = 2^+$ band was proposed by Glatz *et al.* [4], from the theoretical estimate of the intraband $E2$ transition rates, to be consisting of 5292-, 6125-, 7677-, 9542-keV levels of which 5292, 6125, and 9542 keV (identified as 9539 keV) have been observed in the present investigation and found to be de-exciting by 2353-, 833-, and 5221-keV transitions, respectively. The 9539-keV level also de-excites by 3824-keV transition, observed in the present work, as illustrated in the 1004-keV gated spectrum in Fig. 11. These transitions were also known from the previous measurements.

The interband transitions, particularly those feeding the ground-state band, are of significance as they could indicate possible configuration mixing. Similar to Glatz *et al.* [4], the 2523-keV transition from the 4332-keV level of the second 0^+ band, 3667- and 2133-keV transitions respectively from the 5476- and 3943-keV levels of 3^+ band, and 1130- and 2541-keV transitions respectively from the 2939- and 4350-keV levels of the first 2^+ band (based on the 2939-keV level), feeding the 1809-keV level of the ground-state band, have all been observed in the present experiment. Some of the corresponding peaks have been shown in the 1809-keV gated spectrum in Fig. 9. The other interband transition observed with sufficient intensity is 1004 keV, connecting the 3943-keV level of 3^+ band to the 2939-keV level of the 2^+ band. Assignments could be made for the multipolarity and electromagnetic nature of most of these transitions which are in agreement with the previously reported values (Table I).

The level at 4318 keV with $J^\pi = 4^+$ was reported by Glatz *et al.* [4] with exceptional characteristics preventing its assignment to any of the aforesaid rotational sequences. The level was interpreted to be of spherical origin. The state has been observed in the present experiment and found, similar to the previous observations, to be de-exciting by 1379- and 2509-keV transitions. The state at 4839 keV with $J^\pi = 2^+$ (reported as 4835 keV in the previous studies) has been observed in the present measurements. The 896-, 1900-, 3030-keV transitions, previously reported as 893, 1897, and 3026 keV, have also been identified de-exciting the level in the present work.

IV. SHELL-MODEL CALCULATIONS

Shell-model calculations have been carried out to validate the present experimental observations as well as to revisit the previous calculations [4,24] in the light of modified interactions and revised truncation schemes. Calculations have also been extended to the neighboring Mg isotopes and the results have been compared with the available experimental

TABLE II. Average particle occupancies (rounded off to the second decimal) of positive-parity states in ^{26}Mg from shell-model calculations along with the corresponding spectroscopic quadrupole moments and the level lifetimes.

J^π	E_{expt} (keV)	E_{SM} (keV)	Particles	$d_{5/2}$	$d_{3/2}$	$s_{1/2}$	τ (SM) psec	τ (expt.)[a] psec	Q e^2 fm^2
0_1^+	0	0	p	3.19	0.45	0.35	stable	stable	
			n	4.81	0.62	0.55			
2_1^+	1809	1928	p	3.15	0.43	0.41	0.353	0.687 ± 0.017	-14.13
			n	4.70	0.64	0.65			
2_2^+	2939	3153	p	2.98	0.42	0.58	0.165	0.203 ± 0.011	14.58
			n	4.37	0.60	1.02			
0_2^+	3589	3683	p	3.21	0.36	0.42	46.601	9.292 ± 0.202	0.00
			n	3.83	1.37	0.79			
3_1^+	3943	3921	p	3.20	0.39	0.39	3.444	1.226 ± 0.173	26.13
			n	4.45	0.89	0.64			
4_1^+	4318	4528	p	3.40	0.29	0.29	0.211	0.392 ± 0.023	2.93
			n	4.84	0.60	0.55			
2_3^+	4332	4542	p	3.19	0.36	0.44	0.104	0.028 ± 0.040	-15.62
			n	3.83	1.33	0.82			
3_2^+	4350	4511	p	2.99	0.48	0.52	0.111	0.152 ± 0.028	-0.19
			n	4.36	0.62	1.00			
2_4^+	4839	5000	p	3.08	0.37	0.54	0.090	0.040 ± 0.008	6.04
			n	4.38	0.79	0.81			
4_2^+	4901	4930	p	3.04	0.47	0.47	0.049	0.042 ± 0.009	0.69
			n	4.53	0.85	0.61			
0_3^+	4972[a]	5203	p	2.67	0.31	1.00	0.499	0.635 ± 0.086	0.00
			n	4.17	0.78	1.03			
2_5^+	5292	5404	p	3.17	0.43	0.39	0.013	<0.014	18.12
			n	4.48	1.05	0.46			
4_3^+	5476	5470	p	3.00	0.38	0.61	0.039	0.030 ± 0.009	9.52
			n	4.30	0.77	0.91			
1_1^+	5691	5833	p	3.01	0.30	0.67	0.004	<0.011	-0.49
			n	4.32	0.74	0.92			
4_4^+	5715	6006	p	2.81	0.43	0.75	0.055	0.101 ± 0.050	-14.80
			n	4.33	0.71	0.95			
3_3^+	6125	6268	p	3.13	0.42	0.44	0.006	0.020 ± 0.009	4.14
			n	4.46	0.89	0.63			
0_4^+	6256	6067	p	3.12	0.63	0.23	0.106	0.075 ± 0.034	0.00
			n	3.91	0.76	1.32			
4_5^+	6622	6776	p	3.05	0.36	0.57	0.038	0.027 ± 0.007	-22.39
			n	3.82	1.34	0.82			
1_2^+	6634	6799	p	2.99	0.49	0.51	0.005	<0.010	4.43
			n	3.88	1.16	0.95			
2_6^+	6745[a]	6649	p	2.95	0.42	0.62	0.004	0.023 ± 0.011	-1.14
			n	3.96	0.99	1.03			
$(2)_7^+$	6953	6845	p	2.96	0.46	0.56	0.004		-7.12
			n	4.09	0.74	1.16			
4_6^+	6973	7410	p	2.91	0.59	0.49	0.005		25.05
			n	4.16	0.89	0.93			
5_1^+	6978	7035	p	3.11	0.38	0.50	0.029	0.020 ± 0.007	-4.29
			n	4.35	1.00	0.64			
2_8^+	7099	7090	p	2.89	0.59	0.51	0.006	<0.020	13.17
			n	4.49	0.79	0.70			
5_2^+	7395	7462	p	2.86	0.45	0.67	0.016	<0.020	-4.17
			n	4.31	0.61	1.07			
4_7^+	7771	7940	p	3.02	0.46	0.51	0.004	<0.010	-5.62
			n	4.24	1.02	0.72			
6_1^+	8201	8191	p	3.21	0.50	0.28	0.021	<0.020	-0.91
			n	4.51	0.75	0.72			
6_2^+	8472	8424	p	3.27	0.27	0.44	0.030	<0.020	17.87

TABLE II. (*Continued.*)

J^π	E_{expt} (keV)	E_{SM} (keV)	Particles	$d_{5/2}$	$d_{3/2}$	$s_{1/2}$	τ (SM) psec	τ (expt.)[a] psec	Q e^2 fm^2
			n	4.39	0.70	0.89			
5_3^+	8670[a]	8518	p	2.74	0.54	0.71	0.003	<0.010	7.37
			n	4.27	0.77	0.95			
5_4^+	9064[a]	8933	p	2.94	0.58	0.47	0.002	<0.010	7.93
			n	4.35	0.78	0.85			
5_5^+	9539	9453	p	2.65	0.65	0.69	0.007	<0.020	28.94
			n	4.38	0.89	0.71			
7_1^+	9829	9902	p	3.50	0.21	0.28	0.069	0.053 ± 0.014	25.92
			n	4.56	0.60	0.82			

[a]From Ref. [21].

data [21], in order to probe the systematics. The computations have been carried out using the shell-model code NuShellX @ MSU [25]. A model space comprising $1d_{5/2}$, $1d_{3/2}$, $2s_{1/2}$, $1f_{7/2}$, $1f_{5/2}$, $2p_{3/2}$, $2p_{1/2}$ orbitals has been used for the purpose. The interaction used is $sdpfmw$ [26], that has previously been successfully applied to other nuclei in this region [3,13]. Calculations were performed without any adjustments to the single-particle energies. Since unrestricted calculations are computationally prohibitive, the model space has been appropriately truncated for the positive (sd) and the negative (sd and pf) parity states.

A. Calculations for ^{26}Mg

Results of the shell-model calculations for ^{26}Mg are presented in the Tables II–V and illustrated in Fig. 12.

1. Positive-parity states

The ground-state binding energy is calculated to be -105.531 MeV which is in agreement with the experimental value of -105.528 MeV [27]. The positive-parity states are well reproduced by the pure sd ($0\hbar\omega$) configurations, as illustrated in Fig. 12. The particle occupancies are recorded in Table II. The transition probabilities, calculated using the default values for effective charges (Table IV), have been found to be in agreement with the results from Ref. [4].

The spectroscopic quadrupole moment has been used to infer the shape of the nucleus in a given state. It is worth comparing the deformations and the shape changes in the assigned bands of Glatz *et al.* [4], with the current calculations. The ground-state band, comprised of 0_1^+, 2_1^+, 4_2^+, 6_2^+ undergoes a shape evolution from prolate at low spins to vanishing quadrupole moment at 4_2^+ to oblate at higher spins. This corroborates with the spectroscopic quadrupole moments (Q) from the present shell-model calculations, as illustrated in Table II. Recently Hinohara *et al.* [8] have reported their calculations for the ^{26}Mg nucleus based on the CHFB+LQRPA method. It is noteworthy to mention that these results are discrepant with respect to the shell-model calculations of Glatz *et al.* as well as the present work. For instance, Hinohara *et al.* infer the ground state to be an oblate (potential) minimum while the shell-model calculations indicate a prolate shape. Further, since Hinohara *et al.* have limited their discussions to the low-lying deformed states in

TABLE III. Average particle occupancies (rounded off to the second decimal) of negative-parity states in ^{26}Mg from shell-model calculations along with the corresponding level lifetimes.

J^π	E_{expt} (keV)	E_{SM} (keV)	Particles	$d_{5/2}$	$d_{3/2}$	$s_{1/2}$	$f_{7/2}$	$f_{5/2}$	$p_{3/2}$	$p_{1/2}$	τ (SM) psec	τ (expt.)[a] psec
3_1^-	6876[a]	7585	p	2.95	0.57	0.42	0.02	0.01	0.01	0.00		0.123(50)
			n	3.95	0.55	0.53	0.75	0.04	0.14	0.01		
2_1^-	7261	8209	p	2.91	0.55	0.49	0.01	0.01	0.01	0.00		<0.010
			n	3.91	0.55	0.55	0.65	0.04	0.25	0.01		
4_1^-	7283	7695	p	2.97	0.59	0.41	0.02	0.01	0.00	0.00		0.034(11)
			n	4.05	0.53	0.44	0.78	0.02	0.15	0.00		
2_2^-	7543	8861	p	2.94	0.51	0.51	0.01	0.00	0.01	0.00		<0.010
			n	3.46	0.78	0.77	0.58	0.02	0.31	0.04		
5_1^-	7952	7995	p	2.95	0.57	0.43	0.02	0.01	0.00	0.00		0.020(9)
			n	4.04	0.52	0.46	0.84	0.02	0.09	0.00		
3_2^-	8903	8428	p	2.96	0.49	0.48	0.02	0.01	0.01	0.00		
			n	3.61	0.74	0.69	0.63	0.02	0.25	0.01		
6_1^-	9171	9067	p	2.94	0.55	0.47	0.02	0.01	0.00	0.00	0.332	0.037(11)
			n	4.03	0.52	0.47	0.88	0.02	0.06	0.00		

[a]From Ref. [21].

TABLE IV. Transition probabilities in ^{26}Mg from the present shell-model calculations.

J_i^π	$E^i_{\rm expt}$ (keV)	$E^i_{\rm SM}$ (keV)	J_f^π	$E^f_{\rm expt}$ (keV)	$E^f_{\rm SM}$ (keV)	$B(M1)$ $\mu_N^2\times10^{-3}$	$B(E2)$ e^2 fm^4	$B(M1)$ (expt.)[a] $\mu_N^2\times10^{-3}$	$B(E2)$ (expt.)[a] e^2 fm^4
2_1^+	1809	1928	0_1^+	0	0.00	0.00	86.36		$62.61 \pm {}^{4.11}_{3.65}$
2_2^+	2939	3153	2_1^+	1809	1928	137.90	53.07	$170.05 \pm {}^{13.42}_{11.99}$	$27.42 \pm {}^{12.33}_{9.59}$
2_2^+	2939	3153	0_1^+	0	0.00	0.00	3.65		1.78 ± 0.27
0_2^+	3589	3683	2_1^+	1809	1928	0.00	1.05		4.57 ± 0.27
3_1^+	3943	3921	2_2^+	2939	3153	19.43	0.15	$36.69 \pm {}^{7.16}_{5.37}$	<4.11
3_1^+	3943	3921	2_1^+	1809	1928	0.96	0.02	$1.79 \pm {}^{0.46}_{0.35}$	$5.94 \pm {}^{1.37}_{0.91}$
4_1^+	4318	4528	2_2^+	2939	3153	0.00	7.54		
4_1^+	4318	4528	2_1^+	1809	1928	0.00	31.92		20.56 ± 1.14
2_3^+	4332	4542	2_1^+	1809	1928	25.82	3.17	$102.03 \pm {}^{21.48}_{16.11}$	
3_2^+	4350	4511	2_2^+	2939	3153	41.10	143.50	$62.65 \pm {}^{23.27}_{14.32}$	$42.04 \pm {}^{36.10}_{20.65}$
3_2^+	4350	4511	2_1^+	1809	1928	18.21	5.72	$10.74 \pm {}^{3.58}_{2.68}$	$0.22 \pm {}^{0.36}_{0.18}$
2_4^+	4839	5000	3_1^+	3943	3921	0.45	0.36		
2_4^+	4839	5000	2_2^+	2939	3153	34.25	1.04	$202.27 \pm {}^{35.80}_{28.64}$	
2_4^+	4839	5000	2_1^+	1809	1928	0.70	4.79	$2.14 \pm {}^{0.89}_{0.71}$	
4_2^+	4901	4930	2_1^+	1809	1928	0.00	62.36		$77.69 \pm {}^{25.13}_{15.53}$
2_5^+	5292	5404	2_2^+	2939	3153	264.50	0.28		
4_3^+	5476	5470	4_1^+	4318	4528	383.60	10.25	$733.90 \pm {}^{393.80}_{196.90}$	$64.89 \pm {}^{242.21}_{62.15}$
4_3^+	5476	5470	3_1^+	3943	3921	110.80	89.18	$150.36 \pm {}^{89.50}_{46.54}$	$66.26 \pm {}^{68.55}_{31.99}$
4_3^+	5476	5470	2_1^+	1809	1928	0.00	14.85		$5.48 \pm {}^{4.11}_{2.28}$
1_1^+	5691	5833	2_3^+	4332	4542	21.59	12.93		
1_1^+	5691	5833	2_2^+	2939	3153	231.10	3.59		
1_1^+	5691	5833	2_1^+	1809	1928	103.00	4.30		
4_4^+	5715	6006	3_2^+	4350	4511	56.34	40.28	$168.26 \pm {}^{179.00}_{64.44}$	$37.01 \pm {}^{67.63}_{21.02}$
4_4^+	5715	6006	3_1^+	3943	3921	0.56	1.71	$78.76 \pm {}^{84.13}_{28.64}$	$5.02 \pm {}^{13.25}_{3.65}$
4_4^+	5715	6006	2_2^+	2939	3153	0.00	7.46		$23.76 \pm {}^{27.87}_{9.59}$
3_3^+	6125	6268	2_5^+	5292	5404	274.80	114.30		
0_4^+	6256	6067	1_1^+	5691	5833	98.16	0.00		
4_5^+	6622	6776	3_2^+	4350	4511	17.98	0.54	$35.79 \pm {}^{19.69}_{12.53}$	
1_2^+	6634	6799	2_2^+	2939	3153	168.00	0.73		
4_6^+	6973	7410	3_1^+	3943	3921	101.00	0.22		
5_1^+	6978	7035	4_4^+	5715	6006	9.65	1.83	$50.12 \pm {}^{48.33}_{23.27}$	
5_1^+	6978	7035	4_3^+	5476	5470	134.00	65.88	$393.80 \pm {}^{268.50}_{125.30}$	$109.68 \pm {}^{223.93}_{41.13}$
5_1^+	6978	7035	4_1^+	4318	4528	6.33	12.79	$6.80 \pm {}^{6.08}_{2.86}$	$6.85 \pm {}^{19.65}_{5.02}$
2_8^+	7099	7090	2_2^+	2939	3153	11.71	0.45		
5_2^+	7395	7462	4_4^+	5715	6006	396.30	21.93	>264.92	>16.45
4_7^+	7771	7940	4_1^+	4318	4528	45.91	2.29		
6_1^+	8201	8191	4_2^+	4901	4930	0.00	52.60		
6_2^+	8472	8424	5_1^+	6978	7035	27.94	14.56	>161.10	>28.33
5_5^+	9539	9453	4_1^+	4318	4528	0.87	0.07		
7_1^+	9829	9902	6_1^+	8201	8191	127.10	0.82	$213.01 \pm {}^{80.55}_{46.54}$	

[a]From Ref. [4].

^{26}Mg, a detailed comparison with their results could not be carried out. Nevertheless, the γ-soft nature of the nucleus in the ground state and the subsequent shape evolution is evident in all these calculations.

The $K^\pi = 0^+$ band, based on the 3589-keV level, was proposed to be associated with prolate deformation by Glatz *et al*. and also indicated by the Q values of the band members, 0_2^+, 2_3^+, and 4_5^+ (Table II) from the present calculations. As far as the $K^\pi = 3^+$ band is concerned, Glatz *et al*. assigned the levels 3_1^+, 4_3^+, 5_1^+, 6_3^+ to the band and proposed Coriolis mixing with the $K^\pi = 2^+$ band based on the 2939-keV level. Present shell-model calculations reflect an evolution from oblate to

TABLE V. Transition probabilities in ^{26}Mg from the present shell-model calculations.

J_i^π	$E^i_{\rm expt}$ (keV)	$E^i_{\rm SM}$ (keV)	J_f^π	$E^f_{\rm expt}$ (keV)	$E^f_{\rm SM}$ (keV)	$B(M1)$ μ_N^2	$B(E1)/B(E2)$ $e^2\,{\rm fm}^2/e^2\,{\rm fm}^4$
2_1^-	7261	8209	3_1^+	3943	3921	0.00	0.83×10^{-4}
4_1^-	7283	7695	3_1^+	3943	3921	0.00	0.46×10^{-3}
2_2^-	7543	8861	3_1^+	3943	3921	0.00	0.63×10^{-7}
5_1^-	7952	7995	4_1^+	4318	4528	0.00	0.95×10^{-3}
3_2^-	8903	8428	2_1^-	7261	8201	0.03	5.51
6_1^-	9171	9067	5_1^-	7952	7995	0.13	124.10

prolate deformation in the $K^\pi = 3^+$ band, at $J^\pi = 5_1^+$. The $K^\pi = 2^+$ band, assigned to be comprised of 2_2^+, 3_2^+, 4_4^+, 5_2^+, 6_1^+, 7_1^+ levels, was identified to exhibit irregular behavior by Glatz *et al.* which complies with the results of the present calculations.

2. Negative-parity states

The shell-model calculations for the neighboring P nuclei, ^{32,34}P [3,13], have indicated that the negative-parity states in the *sd-pf* nuclei can be generated with a single particle excited to the *fp* shell. Accordingly, the calculations for the negative-parity states in Mg isotopes have been carried out by considering the excitation of a single nucleon from the *sd* to the *fp* orbitals ($1\hbar\omega$). The results for the ^{26}Mg nucleus are presented in Fig. 12. The resulting level energies are in satisfactory agreement with the experimental numbers. Particularly for $J^\pi = 5^-,6^-$, the agreement is at the level of ∼40–100 keV while for lower spins $J^\pi = 3^-,4^-$, it is ∼400–700 keV. As mentioned in the preceding section, the shell-model predictions were useful in resolving the $J^\pi = (2,3)^-$ tentative spin assignment for the level at 7261 keV. The calculated energy for the $J^\pi = 2^-$ is in better agreement with the experimental value ($E_{\rm expt} - E_{\rm theo} \sim 900$ keV) than the calculated energy for $J^\pi = 3^-$, which is far more discrepant. Thus, the level has been assigned a spin parity of $J^\pi = 2^-$. As observed from the particle occupancy for the negative-parity states, these states are dominated by the excitations of the neutrons into the $f_{7/2}$ orbital, with minor contribution from occupation of the $p_{3/2}$ orbital. It is understood that, in principle, the negative-parity states would require both *p* to *sd* as well as *sd* to *fp* excitations. Such configurations could not be simultaneously considered within the present calculations. Nevertheless, reasonable agreement in the level energies has been obtained with *sd* to *fp* excitations, not only in the ^{26}Mg nucleus but in the neighboring isotopes, as shall be discussed in the next section. It can thus be stated that the observed level structure of ^{26}Mg can be adequately described by $0\hbar\omega$ (positive-parity) and $1\hbar\omega$ (negative-parity) configuration beyond the oxygen core.

B. Systematics for Mg isotopes

Shell-model calculations have also been carried out for the neighboring Mg isotopes and the results are illustrated in Figs. 13 and 14, individually, for the even-*A* (^{24,26,28}Mg) and the odd-*A* (^{25,27,29}Mg) Mg isotopes. The experimental energies for Mg isotopes, other than ^{26}Mg, have been adopted from the NNDC database [21]. Of particular importance are the calculations for the negative-parity states, which have been carried out for the first time in these nuclei.

The positive-parity states have been calculated including $0\hbar\omega$ excitations (*sd* configurations) and the results, for $^{24\text{-}29}$Mg, are in satisfactory agreement with the experimental observations, as illustrated in Figs. 13 and 14.

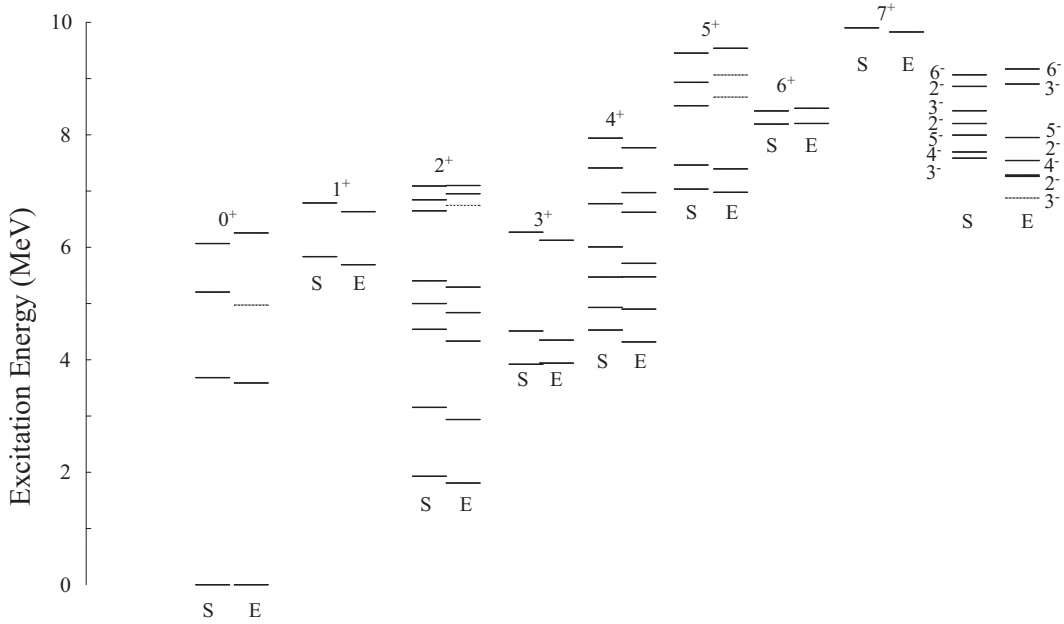

FIG. 12. Calculated levels (denoted by S) in ^{26}Mg shown alongside the experimental levels (denoted by E). Levels that are not observed in the present experiment, but were reported previously and adopted in the NNDC database, are shown in dotted lines. The positive-parity levels have been grouped according to their respective spins, indicated above each group, while the negative-parity levels are drawn in one group.

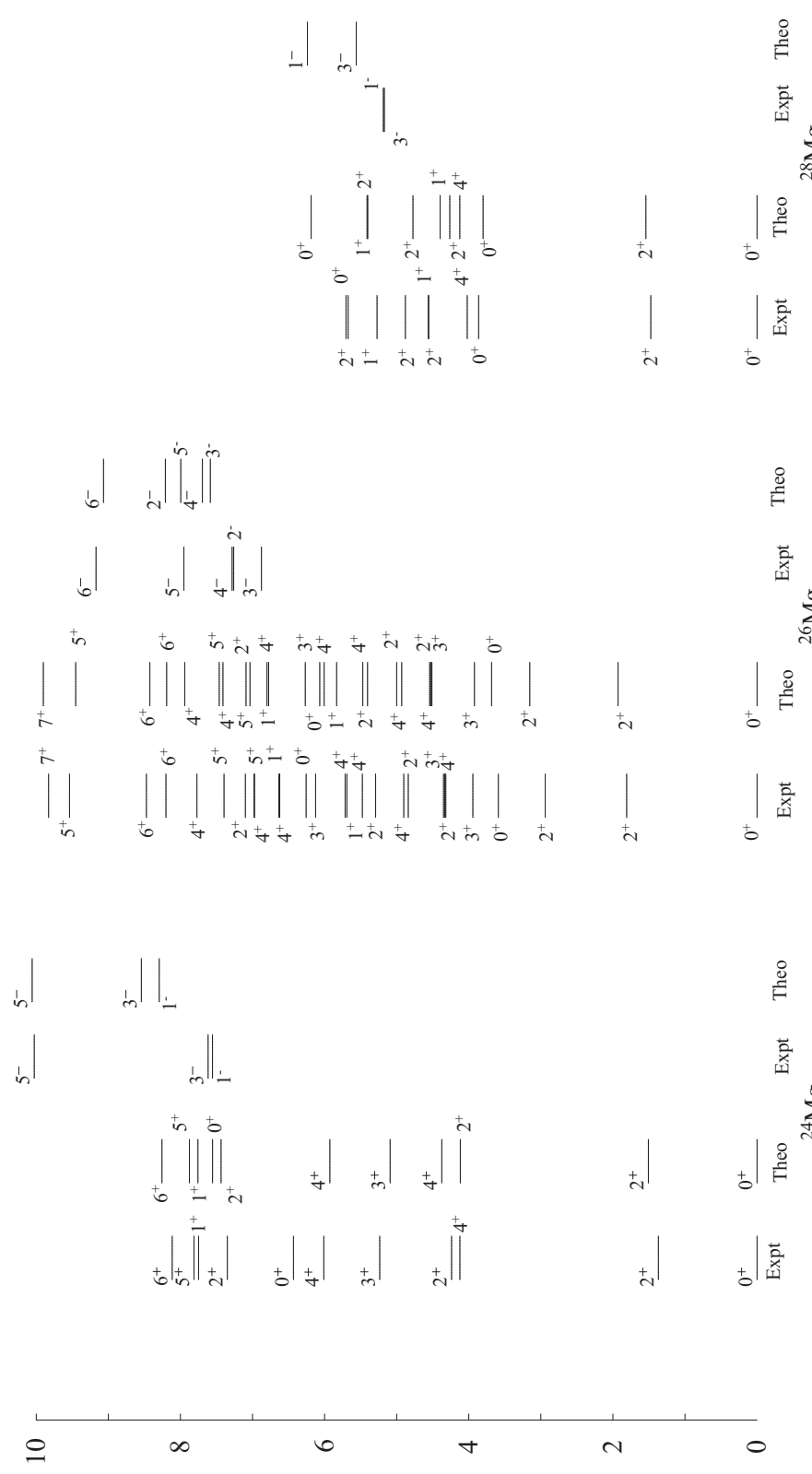

FIG. 13. Comparison of the experimental energy levels (Expt) in even-A Mg isotopes with the shell-model calculations (Theo), carried out in the present work. The data for ^{24,28}Mg are taken from the NNDC database.

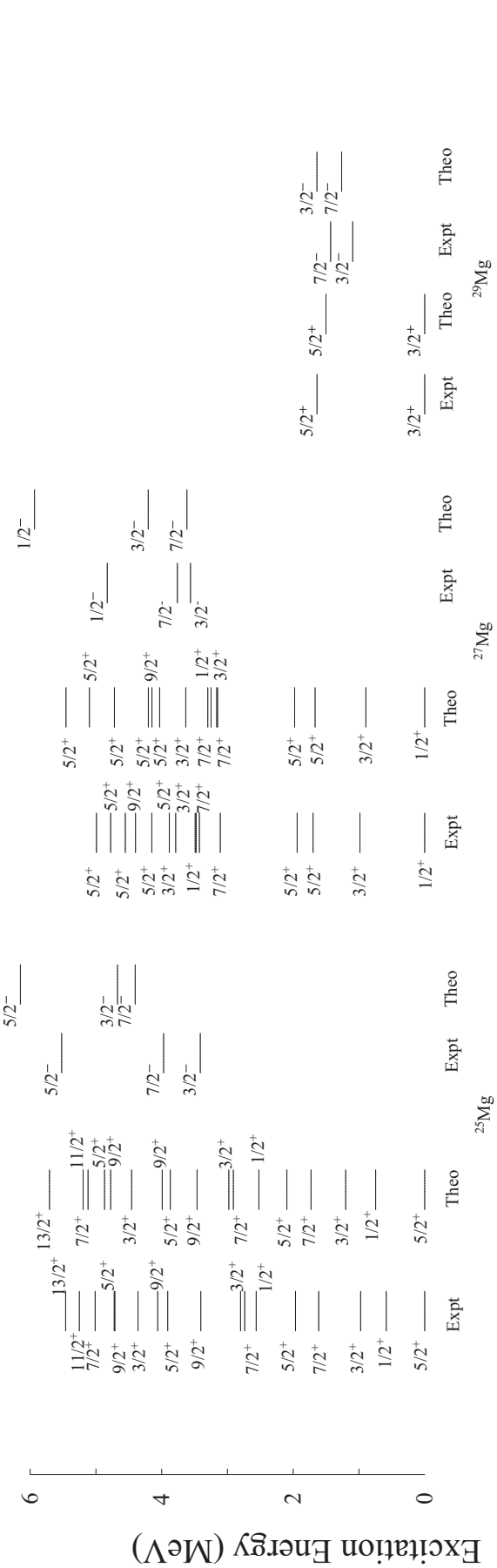

FIG. 14. Comparison of the experimental energy levels (Expt) in odd-A Mg isotopes with the shell-model calculations (Theo), carried out in the present work. The data are taken from the NNDC database.

The negative-parity states in ^{25,27,29}Mg have been calculated including $1\hbar\omega$ excitations. For ^{25}Mg, the agreement with the experimental level energies vary from ∼400 keV for $J^\pi = 7/2^-$ to ∼1.2 MeV for $J^\pi = 3/2^-$. In ^{27}Mg, the tentative spin-parity assignments of $J^\pi = 5/2^-,7/2^-$ on the 3.761-MeV level and $J^\pi = 1/2^-,3/2^-$ on the 4.828 level could be resolved from the present calculations. In case of the former, the shell-model calculations with $J^\pi = 7/2^-$ produced an agreement within ∼150 keV of the experimental value while the predicted energy for $J^\pi = 5/2^-$ is 5.649 MeV, largely discrepant with respect to the experimental level energy, thus favoring the $7/2^-$ assignment to the 3.761-MeV level. For the 4.828 level, calculations with $J^\pi = 1/2^-$, produced an agreement of ∼1.106 MeV while that with $J^\pi = 3/2^-$ was substantially different from the experimental level energy, thus supporting an $1/2^-$ assignment. Similarly, in the case of ^{29}Mg, the present calculations aided in resolving the tentative spin-parity assignments of $J^\pi = 1/2^-,3/2^-$ on the 1.095-MeV level and $J^\pi = 5/2^-,7/2^-$ on the 1.431 level. For the 1.095-keV level, calculations with $J^\pi = 3/2^-$ produced an agreement of ∼−500 keV with the experimental level energy while that for the 1.431-MeV state, with $J^\pi = 7/2^-$, was ∼150 keV. Calculations with alternative spin parities have also been carried out and found to result in substantially discrepant level energies with respect to the experimental results.

The negative-parity states in ^{28}Mg have been calculated including $1\hbar\omega$ excitations. The resulting energies have shown agreement with the experimental energies within ∼400 keV for $J^\pi = 3^-$ and ∼1 MeV for $J^\pi = 1^-$. For the ^{24}Mg nucleus the $J^\pi = 5^-$ level has been well reproduced by $1\hbar\omega$ excitation resulting in an agreement of ∼30 keV, with the experimental level energy. However, for $J^\pi = 1^-$ and 3^- levels of the nucleus $3\hbar\omega$ excitations were necessitated for agreement (∼700–900 keV) with the experimental energy.

It appears that the positive-parity states in the $^{24\text{-}28}$Mg isotopes have been well reproduced within pure *sd* configurations whereas the negative-parity states are dominated by one neutron excitation to the *fp* shell. The calculations were performed without any alteration in the single-particle energy. However, the discrepancy of ∼1 MeV with respect to the experimental data, particularly for the low-lying negative-parity states, might indicate the limitation of the Hamiltonian and omissions of important excitations from *p* to *sd* orbitals that could not be considered in the present calculations.

V. CONCLUSIONS

The level structure of the *sd* shell nucleus, ^{26}Mg, has been investigated for the first time with a heavy-ion-induced fusion-evaporation reaction and a large array of Compton suppressed Clover detectors using γ-γ coincidence measurements. New γ-ray transitions have been observed and placed in the level scheme. Spin-parity assignments of the levels have been made from anisotropy and polarization measurements. The observed level structure has been interpreted within the framework of the spherical shell model using the shell-model code NuShellX @ MSU [25] with the *sdpf* model space, *sdpfmw* interaction

and without any adjustment to the single-particle energies. The positive-parity states are found to be dominated by pure *sd* configurations. The calculations for the negative-parity states, requiring incorporation of *fp* orbitals, have been carried out for the first time, which adequately explained the observed level sequence. The calculations have also been extended, to the neighboring Mg isotopes. The systematics indicate a decrease in the excitation energy of the lowest negative-parity state as a function of increasing neutron number (Figs. 13 and 14) [28,29]. This plausibly indicates the importance of the many-body correlations in favoring the excitation of the nucleons across the conventional shell gaps, and the mixing of the deformation favoring orbitals could stabilize deformed structures at much lower excitation energies than their spherical counterparts.

Finally, it may be commented that the heavy-ion fusion-evaporation reactions are expected to preferentially populate states in the vicinity of the yrast line. However, in the present investigation, several non-yrast states have been observed. This is not commensurate with the general perception. Hence, this observation warrants a detailed investigation of the reaction mechanism to probe the population pattern in the heavy-ion-induced reactions in this mass region.

ACKNOWLEDGMENTS

We thank the staff of the BARC-TIFR Pelletron Linac Facility for their excellent support during the experiment. The help and cooperation of the members of the INGA collaboration in setting up the array is acknowledged. Thanks are due to Mr. Kausik Basu (UGC-DAE CSR, KC), Mr. B. S. Naidu, and Mr. S. Jadhav (TIFR) for their help during the experiment. We are thankful to Mr. J. P. Greene (ANL, USA), Prof. U. Garg, and Nuclear Structure Laboratory, University of Notre Dame for the ^{18}O target. Discussions with Prof. Alex Brown on the shell-model calculations have been of much help and are deeply appreciated. S.S.B. would like to acknowledge the financial assistance (JRF, CSIR Sanction No. 09/838(0038)2010-EMR-I) from the Council of Scientific and Industrial Research (CSIR), Government of India. The INGA Project was partially supported by the Department of Science and Technology, Government of India (Grant No. IR/S2/PF-03/2003-III).

[1] Y. Utsuno, T. Otsuka, T. Mizusaki, and M. Honma, Phys. Rev. C **60**, 054315 (1999).
[2] P. C. Bender *et al.*, Phys. Rev. C **80**, 014302 (2009).
[3] R. Chakrabarti *et al.*, Phys. Rev. C **80**, 034326 (2009).
[4] F. Glatz, S. Norbert, E. Bitterwolf, A. Burkard, F. Heidinger, Th. Kern, R. Lehmann, H. Röpke, J. Siefert, and C. Schneider, Z. Phys. A **324**, 187 (1986).
[5] A. Nagel, G. D. Jones, P. R. G. Lornie, M. R. Nixon, H. G. Price, and P. J. Twin, J. Phys. G **1**, 324 (1975).
[6] A. N. Deacon *et al.*, Phys. Rev. C **82**, 034305 (2010).
[7] D. Seweryniak *et al.*, Phys. Rev. Lett. **94**, 032501 (2005).
[8] N. Hinohara and Y. Kanada-Enyo, Phys. Rev. C **83**, 014321 (2011).
[9] R. Palit *et al.*, Nucl. Instrum. Methods Phys. Res. A **680**, 90 (2012).
[10] Root, http://root.cern.ch/drupal/
[11] S. Saha *et al.*, Phys. Rev. C **86**, 034315 (2012).
[12] D. C. Radford, Nucl. Instrum. Methods Phys. Res. A **361**, 297 (1995).
[13] R. Chakrabarti *et al.*, Phys. Rev. C **84**, 054325 (2011).
[14] P. Singh, R. G. Pillay, J. A. Sheikh, and H. G. Devare, Phys. Rev. C **45**, 2161 (1992).
[15] T. Yamazaki, Nucl. Data A **3**, 1 (1967).
[16] C. Broude and H. E. Gove, Ann. Phys. **23**, 71 (1963).
[17] E. Der Mateosian and A. W. Sunyar, At. Nucl. Data **13**, 391 (1974).
[18] K. Starosta *et al.*, Nucl. Instrum. Methods Phys. Res. A **423**, 16 (1999).
[19] P. M. Jones, L. Wei, F. A. Beck, P. A. Butler, T. Byrski, G. Duchêne, G. de France, F. Hannachi, G. D. Jones, and B. Kharraja, Nucl. Instrum. Methods Phys. Res. A **362**, 556 (1995).
[20] R. Palit, H. C. Jain, P. K. Joshi, S. Nagaraj, B. V. T. Rao, S. N. Chintalapudi, and S. S. Ghugre, Pramana **54**, 347 (2000).
[21] NNDC, URL: www.nndc.bnl.gov
[22] M. Saha Sarkar *et al.*, Nucl. Instrum. Methods Phys. Res. A **556**, 266 (2006).
[23] M. Scheck *et al.*, Phys. Rev. C **83**, 037303 (2011).
[24] W. A. Richter and B. A. Brown, Phys. Rev. C **80**, 034301 (2009).
[25] Nushell @ MSU, B. A. Brown, and W. D. M. Rae, MSU-NSCL Report, 2007.
[26] E. K. Warburton, J. A. Becker, and B. A. Brown, Phys. Rev. C **41**, 1147 (1990).
[27] www.nscl.msu.edu/~brown/resources/SDE.HTM#a26t1
[28] P. Baumann *et al.*, Phys. Rev. C **39**, 626 (1989).
[29] P. M. Endt, Nucl. Phys. A **521**, 1 (1990).